Volume 57
Number 27
7 April 2021
Pages 3297–3420

ChemComm

Chemical Communications

rsc.li/chemcomm

ISSN 1359-7345

ROYAL SOCIETY OF CHEMISTRY

COMMUNICATION

Nikolay Kosinov, Emiel J. M. Hensen *et al.*
Selective methanethiol-to-olefins conversion over HSSZ-13 zeolite

ChemComm

COMMUNICATION

View Article Online
View Journal | View Issue

Cite this: *Chem. Commun.*, 2021, **57**, 3323

Received 22nd January 2021,
Accepted 5th March 2021

DOI: 10.1039/d1cc00397f

rsc.li/chemcomm

Selective methanethiol-to-olefins conversion over HSSZ-13 zeolite†

Miao Yu, Nicoló Tormene, Aleksei Bolshakov, Brahim Mezari, Anna Liutkova, Nikolay Kosinov * and Emiel J. M. Hensen *

A methanethiol-to-olefins (MtTO) equivalent of methanol-to-olefins (MTO) chemistry is demonstrated. CH_3SH can be converted to ethylene and propylene in a similar manner as CH_3OH over SSZ-13 zeolite involving a hydrocarbon pool mechansim. Methylated aromatic intermediates were identified by ^{13}C NMR analysis. Comparison of MtTO and MTO chemistry provides clues about the mechanism of C–C bond formation and catalyst deactivation.

The methanol-to-hydrocarbons (MTH) reaction[1] catalyzed by zeolites represents a promising technology for the conversion of synthesis gas and CO_2 to a variety of chemicals and fuels *via* methanol.[2–4] Intensive investigations into the pathways of the MTH reaction have led to a broad acceptance of the hydrocarbon pool (HCP) mechanism.[5,6] This mechanism involves organocatalytic intermediates of aromatic and olefinic nature, resulting in two catalytic cycles interconnected through hydrogen transfer reactions. The generality of the HCP chemistry is evident from similar mechanistic proposals for the zeolite-catalyzed conversion of methyl halides to higher hydrocarbons,[7] conversion of furanics,[8,9] and the dehydroaromatization of methane.[10] The fact that similar chemistry can arise from different starting reactants prompted us to investigate methanethiol (CH_3SH) substrate. Selective conversion of this industrially important molecule[11] to olefins has not been demonstrated yet.

Earlier work by Chang and Silvestri indicated that CH_3SH can be converted to a mixture of alkanes, heavy aromatics, dimethylsulfide and H_2S on HZSM-5 at 482 °C.[12] Huguet *et al.* reported that conversion of a diluted CH_3SH feed (0.5 kPa in N_2) in the temperature range of 400–550 °C in HZSM-5, HBEA, HFER, HMOR and HSAPO-34 mainly led to CH_4 and H_2S with minor amounts of ethane, propane, and aromatic hydrocarbons.[13,14] Similar to methanol, CH_3SH can also methylate aromatics, *e.g.* toluene to xylenes.[15] The methylation of olefins by CH_3SH can take place over zeolite catalysts as well, although it is significantly more difficult than methylation by CH_3OH.[16] Methylation of aromatics and olefins are important steps in the formation of organocatalytic intermediates in methanol-to-hydrocarbons chemistry.[17] Such computational insights suggest that the conversion of CH_3SH to hydrocarbons *via* the HCP mechanism should be possible over zeolite catalysts.

The conversion chemistry of CH_3SH has been only scarcely investigated in comparison with that of CH_3OH. As it has been noted that CH_3SH readily decomposes into CH_4 and H_2S above 730 °C,[18] we first established a temperature window that would disfavor this unselective gas-phase pathway. For this purpose, we studied the conversion of CH_3SH in a quartz reactor with SiC particles in the temperature range of 350–550 °C (Fig. S1, ESI†), and found that selective catalytic conversion of CH_3SH can only be achieved well below 500 °C where thermal decomposition is avoided. The decomposition products are methane, ethane, dimethylsulfide and heavier organosulfur compounds (Fig. S2, ESI†).

Typical zeolite catalysts that have found utility for the selective conversion of CH_3OH to hydrocarbons are 10MR and 8MR zeolites.[4] The 3-dimensional 10MR micropores of HZSM-5 (MFI topology) can be used to convert CH_3OH to gasoline-range hydrocarbons. When light olefins are targeted, 8MR zeolites like HSSZ-13 (CHA topology) or its aluminophosphate counterpart HSAPO-34 are preferred. We used the CHA and MFI topologies as representative examples of small- and medium-pore zeolites with distinct shape selectivity properties to compare the conversion of CH_3SH and CH_3OH. The basic physico-chemical properties of the used zeolite catalysts are given in Fig. S3–S6 and Tables S1, S2 (ESI†).

The catalytic performance of both zeolites was evaluated at a reactant (CH_3SH or CH_3OH) partial pressure of 6 kPa balanced by N_2 at atmospheric pressure. Based on the non-catalytic experiments with CH_3SH, we selected a temperature of 450 °C for the initial activity evaluation. Fig. 1a shows the CH_3SH and CH_3OH conversion as a function of time on stream. Full conversion of CH_3OH was achieved for HZSM-5 and HSSZ-13

Laboratory of Inorganic Materials and Catalysis, Department of Chemical Engineering and Chemistry, Eindhoven University of Technology, Het Kranenveld 14, 5600 MB, Eindhoven, The Netherlands.
E-mail: n.a.kosinov@tue.nl, e.j.m.hensen@tue.nl

† Electronic supplementary information (ESI) available. See DOI: 10.1039/d1cc00397f

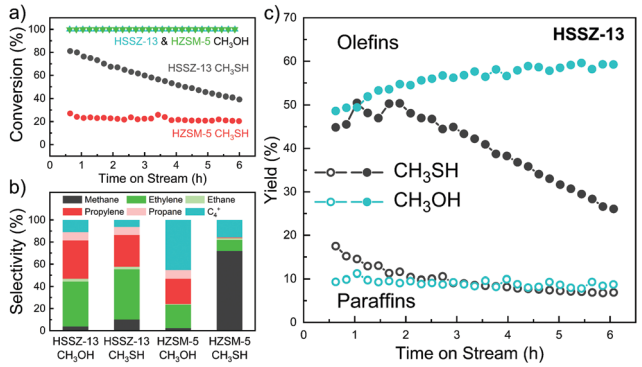

Fig. 1 Catalytic performance of HZSM-5 and HSSZ-13 in conversion of CH_3OH and CH_3SH. (a) Time on stream profiles of CH_3OH/CH_3SH conversion and (b) carbon basis product distributions observed within first 2 h of respective reactions; (c) yield of C_1–C_3 paraffins and C_2–C_3 olefins from CH_3OH and CH_3SH over HSSZ-13. Conditions: 6 kPa of CH_3OH/CH_3SH in N_2 (5 mL min^{-1}), 450 °C, 100 mg of catalysts, 6 h.

during 6 h of time-on-stream. While the CH_3SH conversion on HZSM-5 was low at the start of the reaction (t = 0.5 h, X = 26%), HSSZ-13 achieved a much higher initial conversion of ~80%, which slowly decreased to ~40% after 6 h. The hydrocarbon product distributions obtained within first 2 h on stream are given in Fig. 1b. CH_3OH conversion on HZSM-5 resulted in the expected product slate dominated by light olefins and C_{4+} hydrocarbons and a small amount of CH_4.[19] CH_3SH conversion on HZSM-5 gave mainly CH_4 with minor amounts of C_2H_4 and C_{4+} hydrocarbons. Strikingly, whereas the product distributions for the conversion of CH_3OH and CH_3SH on HZSM-5 were very different, the use of HSSZ-13 offered a comparable hydrocarbon selectivity to light olefins from CH_3SH and CH_3OH. The CH_4 selectivity on HSSZ-13 was slightly higher for CH_3SH. The decreasing CH_3SH conversion with time on stream for HSSZ-13 led to a decreasing yield of light olefins (Fig. 1c) and a higher overall coke selectivity. We also evaluated two other zeolites, HBEA with larger 12MR pores and HFER with interconnected 8MR and 10MR pores. Both zeolites displayed similar poor catalytic performance as HZSM-5 (Fig. S7, ESI†). Among the zeolite topologies evaluated herein, only HSSZ-13 catalyst can selectively produce light olefins. Although the product distribution obtained in the MTO and MtTO reactions over HSSZ-13 are similar, the deactivation rate in the MtTO reaction is higher in combination with a lower initial CH_3SH conversion. These observations can be explained by faster formation of deactivating species and thermodynamic limitations of CH_3SH conversion to olefins and H_2S (90% at the applied conditions).

Next, we studied the influence of the reaction temperature on CH_3SH conversion on HSSZ-13 (Fig. S8, ESI†). At a higher temperature of 500 °C, the unselective decomposition of CH_3SH contributed substantially to the conversion, resulting in a CH_4 hydrocarbon selectivity of 45%. At a lower reaction temperature of 400 °C, the reaction was characterized by an induction period of ~2 h with a product distribution similar to the reaction at 450 °C. The catalytic results suggest that the main catalytic conversion pathways of CH_3OH and CH_3SH are

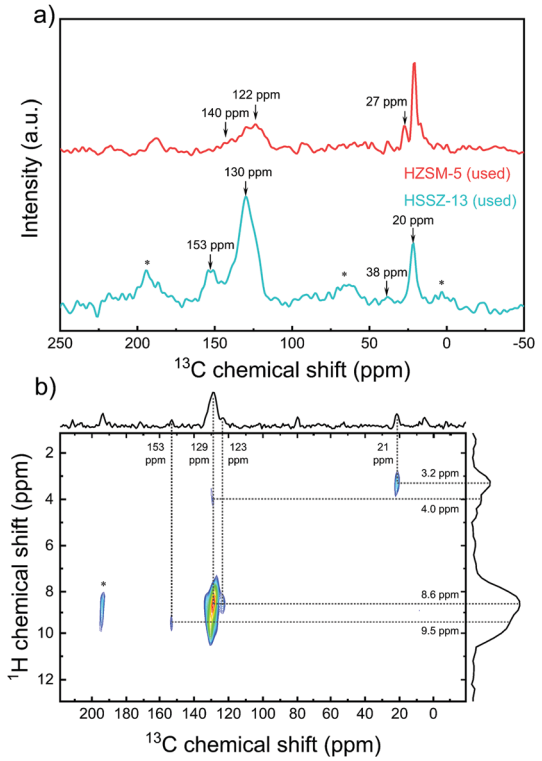

Fig. 2 (a) Direct excitation of ^{13}C NMR spectra of the used HZSM-5 and HSSZ-13 and (b) ^1H-$^{13}C\{^1H\}$ HETCOR MAS NMR 2D spectrum of used HSSZ-13, after 6 h MtTO reaction at 450 °C. Asterisks denote spinning side bands.

similar for the 8MR zeolite HSSZ-13, yet differ for zeolites with larger pores. The induction period observed at a relatively low reaction temperature of 400 °C for CH_3SH conversion is consistent with findings for the MTO reaction.[20,21] As the MTO reaction over HSSZ-13 is known to involve the HCP mechanism, we speculate that such a pool of hydrocarbons is also present in the micropores of HSSZ-13 during the conversion of methanethiol to olefins (MtTO).

We employed ^{13}C MAS NMR spectroscopy to study the organic reaction intermediates occluded in the micropores of the used zeolite catalysts. Direct excitation and cross polarization of ^{13}C NMR spectra of HSSZ-13 and HZSM-5 catalysts after 6 h reaction at 450 °C and 2D ^1H-$^{13}C\{^1H\}$ HETCOR spectrum of the used HSSZ-13 sample are presented in Fig. 2a, Fig. S9 (ESI†) and Fig. 2b, respectively. The ^{13}C NMR spectra feature two main groups of signals at (i) 10–30 ppm, corresponding to sp^3 carbon atoms and (ii) 120–140 ppm, representing sp^2 carbon atoms in arenes and olefins.[22–24] These features are also observed in the 2D HETCOR spectra of the used HSSZ-13 sample. The ^{13}C signal at 129 ppm mainly correlates with the ^1H signal at 8.6 ppm, which indicates arenes to be the main sp^2 carbon species.[25] Considering the intensity differences, the used HSSZ-13 zeolite contained much more aromatic species than the used HZSM-5 sample, which is consistent with the known preference for the aromatic cycle on 8MR zeolites.[22–24]

Furthermore, the NMR spectrum of used HZSM-5 presents a higher relative intensity of sp^3 carbon species (signal ~21 ppm),

implying a higher concentration of saturated hydrocarbons than typically reported during CH_3OH conversion over HZSM-5.[26] We hypothesize that this is due to the formation and deposition of non-volatile thiols, thioethers and oligosulfides on HZSM-5.[27] Interestingly, the signal at 153 ppm in the ^{13}C NMR spectrum of HSSZ-13, which is characteristic for polymethylcyclopentyl cations, has also been reported during CH_3OH conversion on HSSZ-13 and HSAPO-34 and these species are argued to be important reaction intermediates in the pairing mechanism of the aromatic cycle.[28] The NMR spectra of the catalysts used in MtTO do not contain the typical ^{13}C NMR signals between 50 ppm to 80 ppm due to surface methoxy species and trimethyloxonium species observed during CH_3OH conversion.[29] Instead, signals at 38 ppm and 27 ppm were, respectively, observed on HSSZ-13 and HZSM-5. Such ^{13}C NMR signals can be assigned to surface trialkylsulfonium cations (alkyl = methyl or ethyl), which have also been experimentally reported on HZSM-5.[30] Quantum-chemical calculations demonstrated that the trimethylsulfonium cation is stable on HSSZ-13.[31] It can be suggested that trialkylsulfonium might be an intermediate in MtTO in analogy with the proposed role of trimethyloxonium in MTO chemistry.[29] It has actually been proposed that trimethyloxonium might be an important intermediate in the formation of the first C–C bond.[29,32,33] In summary, ^{13}C NMR spectroscopy revealed key differences between HZSM-5 and HSSZ-13 catalysts in the MtTO reaction. First, the ^{13}C NMR spectrum of used HSSZ-13 featured a signal of polymethylcyclopentyl cations, which strongly points to the importance of the aromatic cycle of HCP mechanism. Second, while the ^{13}C NMR spectrum of used HSSZ-13 contains similar bands as typically observed after CH_3OH conversion, the corresponding spectrum of the used HZSM-5 catalyst contains more intense sp^3 carbon signals, suggesting the deposition of saturated non-volatile deposits such as sulfur-containing aliphatics formed during oligomerization of CH_3SH. The formation of such species in the wider HZSM-5 pores might explain the rapid deactivation of this catalyst.

Next, we characterized the used zeolites in more detail with ^{27}Al NMR spectroscopy, TGA-MS and XPS. The ^{27}Al NMR spectra of fresh and used catalysts in Fig. S10 (ESI†) show that dealumination did not occur during the MtTO reaction. Accordingly, the degradation of the zeolite crystals cannot be a reason for the quick deactivation. The TG profiles and normalized MS signals of CO_2 (m/z = 44) and SO_2 (m/z = 64) of used HSSZ-13 and HZSM-5 during heating in 20 vol% O_2 in He are shown in Fig. 3a and d, respectively (data for used HBEA and HFER in Fig. S11, ESI†). The CO_2 and SO_2 MS signals derive from the oxidation of carbon- and sulfur-containing deposits, providing insight into the nature of the coke species deposited during the MtTO reaction. Although HZSM-5 deactivated very fast during the catalytic test and showed much lower conversion levels, the total amount of coke was only 4.7 wt% (Fig. S12, ESI†). The coke content of used HSSZ-13 was much higher (11.6 wt%) and comparable with the coke content of HSSZ-13 after use in the MTO reaction.[34] TGA-MS profiles show similar CO_2 peaks for the HSSZ-13 and HZSM-5 zeolites used in MtTO with a main combustion feature at 500–600 °C, which was also observed and assigned to coke in zeolite micropores formed

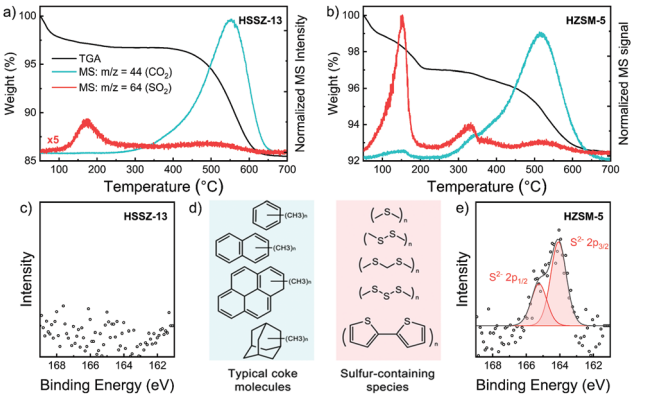

Fig. 3 TGA curves and MS signals of CO_2 (m/z = 44) and SO_2 (m/z = 64) collected under air flow of used (a) HSSZ-13 and (d) HZSM-5. XP spectra of S 2p region of used (b) HSSZ-13 and (e) HZSM-5 (c) typical coke compositions in MTO reaction and potential sulfur-containing coke species in MtTO reaction.

during the MTO reaction and linked to polyolefinic and polyaromatic species (Fig. 3c).[23,35] On the contrary, the SO_2 profiles are different for the two used zeolites. Three contributions can be distinguished: the SO_2 feature below 300 °C is likely related to the decomposition, desorption and combustion of relatively light components having boiling points lower than 300 °C, such as CH_3SH, CH_3SCH_3, and CH_3SSCH_3. The high intensity of the SO_2 signal in comparison with CO_2 suggests that elemental sulfur is present as well. A comparison of this SO_2 feature for the two used zeolites shows that HZSM-5 contains much more of such organosulfur compounds. The second SO_2 peak observed in the range between 300–400 °C appears only in HZSM-5 together with a shoulder in the MS signal of CO_2. Based on its relatively low combustion temperature as compared to typical coke species located inside the pores,[36] we assign this peak to the combustion of heavier sulfur-containing molecules located on the external surface and in near-surface regions of zeolite crystals. Considering that HZSM-5 contains a lower total amount of coke and yet exhibits a lower activity in the MtTO reaction, we argue that these sulfur-containing deposits (Fig. 3c) cause the rapid deactivation of HZSM-5. The third SO_2 peak between 500–600 °C appears together with the large CO_2 peak. Accordingly, we assign this feature to the typical diffusion-limited combustion of coke species confined inside zeolite micropores.[36] The total amount of sulfur-containing species in the used HSSZ-13 catalyst is much smaller than in used HZSM-5.

XPS spectra of used HSSZ-13 and HZSM-5 (Fig. 3b and e) underpin this conclusion. In line with the TG-MS data, no S 2p signals were detected at the surface of used HSSZ-13, whereas clear evidence for the presence of thiols and polysulfides at the surface of the used HZSM-5 zeolite was provided by XPS.[37] For HSSZ-13, the S 2p XPS feature was only observed when the MtTO reaction was carried out at 500 °C (Fig. S13, ESI†). Together with the high CH_4 selectivity observed under these conditions (Fig. S8b, ESI†), we conclude that formation of non-volatile sulfur compounds at the external surface is due to the unselective and non-catalytic decomposition of CH_3SH to CH_4.

Selective conversion of CH_3SH at optimal temperature of 450 °C is related to the sulfur-free HCP aromatics, confined in the SSZ-13 cages.

In conclusion, we demonstrated for the first time the selective conversion of CH_3SH to light olefins and identified HSSZ-13 as a promising catalyst for this novel reaction in the temperature range of 400–450 °C. We established that the HSSZ-13 pores contain aromatic reaction intermediates that have earlier been linked to the aromatic cycle of the MTH reaction. The specific pore geometry of this zeolite (small 8MR windows connecting larger cages) allows formation of the HCP intermediates essential for the selective conversion of CH_3SH to light olefins, but prevents reactions that give rise to bulky deposits that quickly deactivate the near-surface regions of zeolite crystals with larger 10MR and 12MR pores. Next, the main finding of this work that CH_3SH can undergo similar chemistry as CH_3OH can provide clues about the much-debated aspects of MTH chemistry such as the formation of the first C–C bond and the deactivation mechanism. Formaldehyde formed by disproportionation of CH_3OH can alkylate olefinic and aromatic chain growth carriers, accelerating the relative rates of hydrogen transfer and thus the transformation of active HCP intermediates into deactivating species.[38,39] Moreover, formaldehyde has been implicated in the chemistry leading to the formation of the first C–C bond.[40,41] CO derived from CH_3OH decomposition can be involved in Koch-type carbonylation of methoxy species or dimethyl-ether to form the first C–C bond. While both routes are not feasible with CH_3SH (*i.e.*, carbon monosulfide CS and thioformaldehyde CH_2S are not stable under the applied conditions), the presented MtTO reaction still exhibits common characteristics of MTH chemistry such as C–C bond formation and deactivation. It is therefore worthwhile to investigate these aspects in more detail. The finding that HSSZ-13 zeolite can convert CH_3SH with a hydrocarbon selectivity to light olefins close to the selectivity observed for MTO opens a new research direction for optimizing 8MR zeolites towards valorization of CH_3SH into valuable chemical building blocks. Further mechanistic studies, including density functional theory calculations, spectroscopy and isotope labelling, will shed light on the dominant reaction pathways of MtTO chemistry. Finally, reaction optimization including other 8MR zeotypes such as silicoaluminophosphates with milder acidity (*e.g.* SAPO-34) and hierarchically porous zeolites will undoubtedly lead to improved MtTO performance.

Conflicts of interest

There are no conflicts to declare.

Notes and references

1 S. L. Meisel, J. P. McCullough, C. H. Lechthaler and P. B. Weisz, *Chem. Tech.*, 1976, **6**, 86–89.
2 X. Niu, J. Gao, Q. Miao, M. Dong, G. Wang, W. Fan, Z. Qin and J. Wang, *Microporous Mesoporous Mater.*, 2014, **197**, 252–261.
3 M. Conte, J. A. Lopez-Sanchez, Q. He, D. J. Morgan, Y. Ryabenkova, J. K. Bartley, A. F. Carley, S. H. Taylor, C. J. Kiely, K. Khalid and G. J. Hutchings, *Catal. Sci. Technol.*, 2012, **2**, 105–112.
4 U. Olsbye, S. Svelle, M. Bjrgen, P. Beato, T. V. W. Janssens, F. Joensen, S. Bordiga and K. P. Lillerud, *Angew. Chem., Int. Ed.*, 2012, **51**, 5810–5831.
5 I. M. Dahl and S. Kolboe, *J. Catal.*, 1994, **149**, 458–464.
6 I. M. Dahl and S. Kolboe, *J. Catal.*, 1996, **161**, 304–309.
7 S. Svelle, S. Aravinthan, M. Bjørgen, K. P. Lillerud, S. Kolboe, I. M. Dahl and U. Olsbye, *J. Catal.*, 2006, **241**, 243–254.
8 E. A. Uslamin, H. Saito, N. Kosinov, E. Pidko, Y. Sekine and E. J. M. Hensen, *Catal. Sci. Technol.*, 2020, **10**, 2774–2785.
9 E. A. Uslamin, N. Kosinov, G. A. Filonenko, B. Mezari, E. Pidko and E. J. M. Hensen, *ACS Catal.*, 2019, **9**, 8547–8554.
10 N. Kosinov, A. S. G. Wijpkema, E. Uslamin, R. Rohling, F. J. A. G. Coumans, B. Mezari, A. Parastaev, A. S. Poryvaev, M. V. Fedin, E. A. Pidko and E. J. M. Hensen, *Angew. Chem., Int. Ed.*, 2018, **57**, 1016–1020.
11 W. Leuchtenberger, K. Huthmacher and K. Drauz, *Appl. Microbiol. Biotechnol.*, 2005, **69**, 1–8.
12 C. D. Chang and A. J. Silvestri, *J. Catal.*, 1977, **47**, 249–259.
13 E. Huguet, B. Coq, R. Durand, C. Leroi, R. Cadours and V. Hulea, *Appl. Catal., B*, 2013, **134–135**, 344–348.
14 V. Hulea, E. Huguet, C. Cammarano, A. Lacarriere, R. Durand, C. Leroi, R. Cadours and B. Coq, *Appl. Catal., B*, 2014, **144**, 547–553.
15 C. Cammarano, E. Gay, A. Finiels, O. Fajula and V. Hulea, *ACS Catal.*, 2019, **9**, 605–609.
16 Q. M. Li, M. Zhang, C. M. Wang, Y. A. Zhu, X. G. Zhou and Z. K. Xie, *Mol. Catal.*, 2018, **446**, 106–114.
17 S. Svelle, U. Olsbye, F. Joensen and M. Bjørgen, *J. Phys. Chem. C*, 2007, **111**, 17981–17984.
18 A. H. Sehon and B. D. Darwent, *J. Am. Chem. Soc.*, 1954, **76**, 4806–4810.
19 M. Bjørgen, S. Svelle, F. Joensen, J. Nerlov, S. Kolboe, F. Bonino, L. Palumbo, S. Bordiga and U. Olsbye, *J. Catal.*, 2007, **249**, 195–207.
20 E. Borodina, H. Sharbini Harun Kamaluddin, F. Meirer, M. Mokhtar, A. M. Asiri, S. A. Al-Thabaiti, S. N. Basahel, J. Ruiz-Martinez and B. M. Weckhuysen, *ACS Catal.*, 2017, **7**, 5268–5281.
21 E. Borodina, F. Meirer, I. Lezcano-González, M. Mokhtar, A. M. Asiri, S. A. Al-Thabaiti, S. N. Basahel, J. Ruiz-Martinez and B. M. Weckhuysen, *ACS Catal.*, 2015, **5**, 992–1003.
22 C. Wang, J. Xu and F. Deng, *ChemCatChem*, 2020, **12**, 965–980.
23 E. Epelde, M. Ibañez, A. T. Aguayo, A. G. Gayubo, J. Bilbao and P. Castaño, *Microporous Mesoporous Mater.*, 2014, **195**, 284–293.
24 D. Fu, A. Lucini Paioni, C. Lian, O. van der Heijden, M. Baldus and B. M. Weckhuysen, *Angew. Chem., Int. Ed.*, 2020, **59**, 20024–20030.
25 W. Dai, C. Wang, M. Dyballa, G. Wu, N. Guan, L. Li, Z. Xie and M. Hunger, *ACS Catal.*, 2015, **5**, 317–326.
26 A. Dutta Chowdhury, I. Yarulina, E. Abou-Hamad, A. Gurinov and J. Gascon, *Chem. Sci.*, 2019, **10**, 8946–8954.
27 F. Freeman and C. N. Angeletakis, *Org. Magn. Reson.*, 1983, **21**, 86–93.
28 S. Xu, A. Zheng, Y. Wei, J. Chen, J. Li, Y. Chu, M. Zhang, Q. Wang, Y. Zhou, J. Wang, F. Deng and Z. Liu, *Angew. Chem., Int. Ed.*, 2013, **52**, 11564–11568.
29 X. Wu, S. Xu, W. Zhang, J. Huang, J. Li, B. Yu, Y. Wei and Z. Liu, *Angew. Chem., Int. Ed.*, 2017, **56**, 9039–9043.
30 E. J. Munson, A. A. Kheir and J. F. Haw, *J. Phys. Chem.*, 1993, **97**, 7321–7327.
31 J. Baltrusaitis, T. Bučko, W. Michaels, M. Makkee and G. Mul, *Appl. Catal., B*, 2016, **187**, 195–203.
32 E. J. Munson, A. A. Kheir, N. D. Lazo and J. F. Haw, *J. Phys. Chem.*, 1992, **96**, 7740–7746.
33 E. J. Munson and J. F. Haw, *J. Am. Chem. Soc.*, 1991, **113**, 6303–6305.
34 X. Zhu, J. P. Hofmann, B. Mezari, N. Kosinov, L. Wu, Q. Qian, B. M. Weckhuysen, S. Asahina, J. Ruiz-Martínez and E. J. M. Hensen, *ACS Catal.*, 2016, **6**, 2163–2177.
35 J. Li, G. Xiong, Z. Feng, Z. Liu, Q. Xin and C. Li, *Microporous Mesoporous Mater.*, 2000, **39**, 275–280.
36 N. Kosinov, E. A. Uslamin, F. J. A. G. Coumans, A. S. G. Wijpkema, R. Y. Rohling and E. J. M. Hensen, *ACS Catal.*, 2018, **8**, 8459–8467.
37 J. Riga and J. J. Verbist, *J. Chem. Soc., Perkin Trans. 2*, 1983, 1545–1551.
38 A. Hwang, M. Kumar, J. D. Rimer and A. Bhan, *J. Catal.*, 2017, **346**, 154–160.
39 A. Hwang and A. Bhan, *Acc. Chem. Res.*, 2019, **52**, 2647–2656.
40 A. D. Chowdhury, K. Houben, G. T. Whiting, M. Mokhtar, A. M. Asiri, S. A. Al-Thabaiti, S. N. Basahel, M. Baldus and B. M. Weckhuysen, *Angew. Chem., Int. Ed.*, 2016, **55**, 15840–15845.
41 Y. Liu, S. Müller, D. Berger, J. Jelic, K. Reuter, M. Tonigold, M. Sanchez-Sanchez and J. A. Lercher, *Angew. Chem., Int. Ed.*, 2016, **55**, 5723–5726.

